



**HAL**  
open science

## Numerical modelling of salt leaching-dissolution process

Farid Laouafa, Jianwei Guo, Michel Quintard, Haishan Luo

► **To cite this version:**

Farid Laouafa, Jianwei Guo, Michel Quintard, Haishan Luo. Numerical modelling of salt leaching-dissolution process. 49. US Rock Mechanics / Geomechanics Symposium, Jun 2015, San Francisco, CA, United States. ineris-01855079

**HAL Id: ineris-01855079**

**<https://ineris.hal.science/ineris-01855079>**

Submitted on 4 Sep 2018

**HAL** is a multi-disciplinary open access archive for the deposit and dissemination of scientific research documents, whether they are published or not. The documents may come from teaching and research institutions in France or abroad, or from public or private research centers.

L'archive ouverte pluridisciplinaire **HAL**, est destinée au dépôt et à la diffusion de documents scientifiques de niveau recherche, publiés ou non, émanant des établissements d'enseignement et de recherche français ou étrangers, des laboratoires publics ou privés.

# Numerical modelling of salt leaching-dissolution process

F. LAOUAFA

Institut National de l'Environnement Industriel et des Risques- INERIS, F-60550 Verneuil-en-Halate, France

J. GUO

Université de Toulouse ; INPT, UPS, IMFT (Institut de Mécanique des Fluides de Toulouse), Allée Camille Soula, F-31400 Toulouse, France

M. QUINTARD

Université de Toulouse ; INPT, UPS ; IMFT (Institut de Mécanique des Fluides de Toulouse), Allée Camille Soula, F-31400 Toulouse, France & CNRS ; IMFT, F-31400 Toulouse, France

H. LUO

Université de Toulouse ; INPT, UPS, IMFT (Institut de Mécanique des Fluides de Toulouse), Allée Camille Soula, F-31400 Toulouse, France

**ABSTRACT:** Extraction of salt by leaching process is used intensively nowadays. This process extracts salt by dissolving the mineral with water. In this analysis about cavity dissolution modeling, we consider the case of a binary system, i.e., a chemical solute corresponding to the solid that is dissolved by a “solvent” (mainly water). Rock salt dissolution is controlled by thermodynamic equilibrium at the interface, i.e., equality of the chemical potentials. In this paper, a local non-equilibrium Diffuse Interface Model (DIM) and an explicit treatment of the brine-salt interface (using an ALE (Arbitrary Lagrangian-Eulerian) technique) are introduced in order to solve such dissolution problems. The control equations are obtained by upscaling micro-scale equations for a solid-liquid dissolution problem using a volume averaging theory. Based on this mathematical formulation, dissolution test cases are presented. We introduce and discuss the main features of the method. Illustrations of the interaction between natural convection and forced convection in dissolution problems are presented and the time and space evolution of the rock salt-fluid interface is shown through several examples.

## 1. INTRODUCTION

Dissolution of porous media or solids is widely concerned in many industrial fields, e.g., acid injection into petroleum reservoirs, dissolution of rocks caused by underground water, etc. In the latter, rock dissolution creates underground cavities of different shapes and sizes, which induces a potential risk of collapse as shown in Fig.1. In most applications, modeling such liquid/solid dissolution problems is of paramount importance.



Fig 1 Land Subsidence in Central Kansas Related to Salt dissolution

Among all methods used for modeling dissolution process, we present two ways for simulating this problem. The first one is a direct treatment of the

evolution of the fluid-solid interface, for instance using an ALE (Arbitrary Lagrangian-Eulerian) method [4]. The second uses a Diffuse Interface Model (DIM) to smooth the interface with continuous quantities [1, 3, 6], like the liquid phase volume fraction, species mass fractions, etc.

However, there are several difficulties associated with ALE method for the dissolution problem: in particular, the need for fine meshes near the dissolving interface can lead to severely deformed grid elements inducing numerical problems (instabilities, need for remeshing, etc.).

On the contrary, it is easier to implement a DIM model because of the smoothing of the interface singularity, and resulting codes are more numerically stable and more efficient. In a previous study, Golfier et al. [5] showed that a non-equilibrium Darcy-scale model was a good candidate for a DIM dissolution model. In their work, the Darcy-scale balance equations were obtained by averaging small-scale (micro-scale) equations, with the help of the volume averaging theory as introduced by Whitaker [12]. In particular, it was able to capture the instability pattern such as wormhole during the dissolution of a porous medium, which is known to be a very difficult numerical problem. Their results showed that this non-equilibrium model can also be used to

simulate local equilibrium states which are reminiscent of the original dissolution problem. Therefore, it can be used as a diffuse interface model to simulate dissolution problems instead of explicit tracking of the dissolution interface (such as in ALE frameworks).

In this previous work, density gradients induced by spatial variations of concentration were neglected. Indeed Golfier et al. [5] model considers the liquid phase species only as a tracer.

For most problems, for instance cavity in salt formations, we may have very high concentration gradient due to the high solubility of salt around the solid/liquid interface. Neglecting strong density gradients may bring inaccuracy to the prediction of dissolution. This may be the case with salt formations since the solubility of salt is around 360 g/l in comparison with that of gypsum which is about 2.6 g/l.

Consequently, the density gradient should be considered for an accurate analysis. In this paper, a Darcy-scale diffuse interface model (DIM) including density driven flows is deduced from the original liquid/solid dissolution in the case of a binary system (following Golfier et al. [5]). For a first study about cavity dissolution modeling, we consider the case of a binary system, i.e., a chemical solute constitutes the solid that is dissolved by a “solvent” (mainly water in most practical applications).

The balance equations, which include the mass balance equations for the  $\beta$  (fluid) and  $\sigma$  (rock salt solid) phases, and species in the  $\beta$ -phase, are obtained in the form of two partial differential-equation models, with an exchange term between the  $\beta$ -phase and  $\sigma$ -phase.

In the next section, the original model is introduced and the corresponding Darcy-scale model is obtained with the help of an averaging theory. In the following sections, several numerical simulations are presented. Comparison between the results using either ALE or DIM shows good agreement. Then we show the ability of the DIM model to deal with complex problems: salt fingering phenomena resulting from fluid flow instability, in-situ scale modeling and comparison of kinetic dissolution and shape for salt and gypsum.

## 2. DISSOLUTION MODEL

Two types of dissolution model are considered. The original dissolution problem is illustrated in Figure 2 for a binary system. The solid/liquid interface is described mathematically by a surface at which the liquid concentration is equal to an equilibrium concentration. If we introduce a scalar phase indicator,  $\mathcal{E}_\beta$  (volume fraction of the  $\beta$ -phase, porosity), it has a value of 1 in the liquid and zero elsewhere, as illustrated in Figure 2.

Solving a dissolution problem requires a special front tracking numerical technique, which is often computationally time consuming. Alternative models do not require an explicit treatment of the moving interface. Instead, partial differential equations are written for  $\mathcal{E}_\beta$  and the concentration  $\omega_{A\beta}$  (masse fraction of species A in the phase  $\beta$ ), which lead to a diffuse interface as illustrated in Figure 2. We will present below the two formulations.

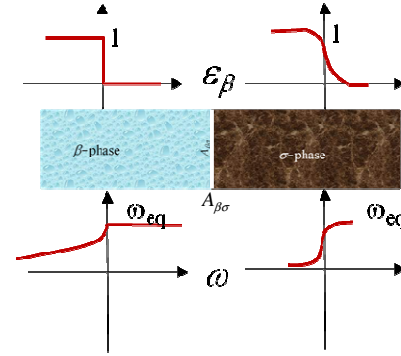


Fig. 2 . Original dissolution (sharp interface on the left) and Diffuse Interface Model (on the right).

The original solid/liquid dissolution problem can be described by classical convective-diffusive mass balance and Navier-Stokes equations, etc. To express the DIM model, we start from these original solid/liquid equations to generate Darcy-scale equations, the corresponding Darcy-scale quantities and effective coefficients, with the help of the volume averaging theory [12], and taking into account the density function of concentration. In the first subsection, the original model for the dissolution problem is introduced. In the second subsection, we present the upscaling method leading to the “Darcy-scale” equations.

### 2.1 The original multiphase model

We consider a binary liquid phase  $\beta$  containing chemical species A and B, and a solid phase  $\sigma$  containing only chemical species A.

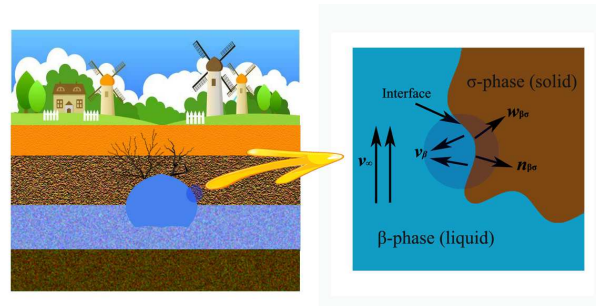


Fig. 3: In-situ induced problem by dissolution (left) and explanation of the variables at the local level to the interface (right).

In Figure 3,  $\mathbf{v}_\infty, \mathbf{v}_\beta, \mathbf{w}, \mathbf{n}_{\beta\sigma}$  represent the velocity of the fluid far away from the interface, the speed of the phase  $\beta$  near the interface, the recession rate, and the normal to the interface, respectively. In the following, bold letters indicates either vector or tensor variables.

We write the different balance equations below. The total mass balance equation for the  $\beta$ -phase is

$$\frac{\partial \rho_\beta}{\partial t} + \nabla \cdot (\rho_\beta \mathbf{v}_\beta) = 0 \quad (1)$$

The mass balance equations for **species A and B** in the  $\beta$ -phase are written as,

$$\frac{\partial (\rho_\beta \omega_{A\beta})}{\partial t} + \nabla \cdot (\rho_\beta \omega_{A\beta} \mathbf{v}_{A\beta}) = 0 \quad (2)$$

$$\frac{\partial (\rho_\beta \omega_{B\beta})}{\partial t} + \nabla \cdot (\rho_\beta \omega_{B\beta} \mathbf{v}_{B\beta}) = 0 \quad (3)$$

where  $\omega_{A\beta}$  and  $\omega_{B\beta}$  represent the mass fractions of species A and B, respectively. The general mass balance equation for a moving  $\sigma$ -phase is written as

$$\frac{\partial \rho_\sigma}{\partial t} + \nabla \cdot (\rho_\sigma \mathbf{v}_\sigma) = 0 \quad (4)$$

In the case of the fluid, we will use the Navier-Stokes equations. This set of equations is recalled below for the  $\beta$ -phase.

$$\rho_\beta \left( \frac{\partial \mathbf{v}_\beta}{\partial t} + \mathbf{v}_\beta \cdot \nabla \mathbf{v}_\beta \right) = \rho_\beta \mathbf{g} - \nabla P_\beta + \mu_\beta \nabla^2 \mathbf{v}_\beta \quad (5)$$

where  $\mathbf{v}_\beta$  represents the velocity of the  $\beta$ -phase,  $\nabla P_\beta$  the pressure gradient in the  $\beta$ -phase,  $\mu_\beta$  the viscosity of the  $\beta$ -phase and  $\mathbf{g}$  the gravity. At the  $\beta$ - $\sigma$  interface  $A_{\beta\sigma}$ , the chemical potentials for each species should be equal for the different phases. Therefore, for the special binary case under investigation, we have the following equality at a given pressure  $P$  and temperature  $T$ :

$$\mu_{A\beta}(\omega_{A\beta}, P, T) = \mu_{A\sigma}(\omega_{A\sigma}, P, T) \quad \text{at } A_{\beta\sigma} \quad (6)$$

where  $\omega_{A\beta}$  is equal to 1. It must be emphasized that in the complete binary case, i.e., when  $\omega_{A\beta}$  is not equal to 1, there is also a relation similar to the above equation for the other components.

This results is a classical equilibrium condition imposing an equilibrium concentration ( $\omega_{eq}$ ) for species A, i.e.,

$$\omega_{A\beta} = \omega_{eq} \quad \text{at } A_{\beta\sigma}$$

We deduce from the mass balances for species A and B the following relations at the  $\beta$ - $\sigma$  interface:

$$\rho_\beta \omega_{A\beta} (\mathbf{v}_{A\beta} - \mathbf{w}) \cdot \mathbf{n}_{\beta\sigma} = \rho_\sigma \omega_{A\sigma} (\mathbf{v}_{A\sigma} - \mathbf{w}) \cdot \mathbf{n}_{\beta\sigma} \quad \text{at } A_{\beta\sigma} \quad (7)$$

$$\rho_\beta \omega_{B\beta} (\mathbf{v}_{B\beta} - \mathbf{w}) \cdot \mathbf{n}_{\beta\sigma} = \rho_\sigma \omega_{B\sigma} (\mathbf{v}_{B\sigma} - \mathbf{w}) \cdot \mathbf{n}_{\beta\sigma} \quad \text{at } A_{\beta\sigma}$$

And the following expression for the total mass balance at the  $\beta$ - $\sigma$  interface gives:

$$\rho_\beta (\mathbf{v}_\beta - \mathbf{w}) \cdot \mathbf{n}_{\beta\sigma} = \rho_\sigma (\mathbf{v}_\sigma - \mathbf{w}) \cdot \mathbf{n}_{\beta\sigma} \quad \text{at } A_{\beta\sigma} \quad (8)$$

where  $\mathbf{w}$  represents the velocity of the interface with  $\mathbf{n}_{\beta\sigma}$  the interface normal, and we have  $\mathbf{v}_\sigma = \mathbf{v}_{A\sigma}$ . Let us underline that only two of these three latter equations are independent. From the above equations and using a theory of diffusion [11], we have:

$$\rho_\beta \omega_{A\beta} \mathbf{v}_{A\beta} = \rho_\beta \omega_{A\beta} \mathbf{v}_\beta - \rho_\beta D_{A\beta} \nabla \omega_{A\beta} \quad (9)$$

Then,

$$\rho_\beta \omega_{A\beta} (\mathbf{v}_{A\beta} - \mathbf{w}) \cdot \mathbf{n}_{\beta\sigma} = \quad (10)$$

$$\mathbf{n}_{\beta\sigma} \cdot (\rho_\beta \omega_{A\beta} (\mathbf{v}_\beta - \mathbf{w}) - \rho_\beta D_{A\beta} \nabla \omega_{A\beta}) \quad \text{at } A_{\beta\sigma}$$

The mass balance for species A, can then be expressed as follow:

$$\frac{\partial (\rho_\beta \omega_{A\beta})}{\partial t} + \nabla \cdot (\rho_\beta \omega_{A\beta} \mathbf{v}_\beta) = \nabla \cdot (\rho_\beta D_{A\beta} \nabla \omega_{A\beta}) \quad (11)$$

The whole balance equations presented above are sufficient to solve the physical problem, provided that the overall surrounding boundary conditions are also given. After some equation transformations we have the two following expressions:

$$\mathbf{n}_{\beta\sigma} \cdot \mathbf{v}_\beta = \mathbf{n}_{\beta\sigma} \cdot \left( \mathbf{v}_\sigma + \frac{\rho_\beta - \rho_\sigma}{\rho_\sigma (1 - \omega_{A\beta})} D_{A\beta} \nabla \omega_{A\beta} \right) \quad \text{at } A_{\beta\sigma} \quad (12)$$

$$\mathbf{n}_{\beta\sigma} \cdot \mathbf{w} = \mathbf{n}_{\beta\sigma} \cdot \left( \mathbf{v}_\sigma + \frac{\rho_\beta}{\rho_\sigma (1 - \omega_{A\beta})} D_{A\beta} \nabla \omega_{A\beta} \right) \quad \text{at } A_{\beta\sigma} \quad (13)$$

where  $D_{A\beta}$  represents the diffusion coefficient.

It is this last formula which expresses explicitly the recession velocity used for an explicit computation of the interface (e.g. ALE). The flux balance for the different species at the interface is described by various equations. It is important to note that it is on the basis of these expressions that we construct the recession velocity of the interface and thus the dissolution rate. The dissolution problem should be completed with the

set of equations to describe the boundary conditions of the fluid domain (because this one is transient).

The simulation of the dissolution process has been implemented in the ALE frameworks using the above analysis, in which the location of the interface moves accordingly.

As it is well-known, the dissolution process can lead to very sharp fronts at some points of the interface, and lead to huge numerical difficulties. We can circumvent them by using a Diffuse Interface Method, which is very suitable for such analysis. Contrary to "sharp methods" which consider the interface between the two phases as a discontinuous surface, a diffuse interface method considers the interface as a transition layer where the quantities vary rapidly but smoothly. The whole domain constituted by the two phases is considered to be a continuous medium without any singularities nor strict distinction of solid or liquid, etc. (see Figure 2).

Neglecting the density variation, Golfier et al. [5] studied one example of a diffuse interface model. This is a non-equilibrium dissolution model that gives a diffuse interface model depending on a mass exchange coefficient  $\alpha$ .

It has the ability to be very close, with a proper choice of the exchange term (i.e.,  $\alpha$ ) to the local equilibrium solution, which is equivalent to the original dissolution problem.

Based on Golfier et al. [5] work, we develop, in the following subsection, a diffuse interface method under the form of a Darcy-scale dissolution model considering the effect of density variation.

## 2.2 Darcy non-equilibrium model

In our case, the  $\sigma$ -phase is immobile. Therefore, we have  $\mathbf{v}_\sigma = 0$  in the following analysis.

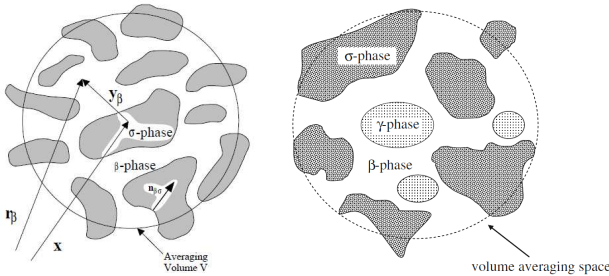


Fig. 4. Averaging volume at pore scale level and material point position vector (left) and 3-phases model (the third phase may be insoluble species for instance) (right).

The volume averaging theory [10, 12] will be used to upscale the balance equations formulated at the pore scale (Figure 4). The averaged form of balance equation of species A can be expressed as:

$$\frac{\partial \langle \rho_\beta \omega_{A\beta} \rangle}{\partial t} + \nabla \cdot \langle \rho_\beta \omega_{A\beta} \mathbf{v}_{A\beta} \rangle = -\frac{1}{V} \int_{A_{\beta\sigma}} \mathbf{n}_{\beta\sigma} \cdot \rho_\beta \omega_{A\beta} (\mathbf{v}_{A\beta} - \mathbf{w}) \quad (14)$$

The above equation can then be transformed as:

$$\underbrace{\frac{\partial \langle \rho_\beta \omega_{A\beta} \rangle}{\partial t}}_{(a)} + \underbrace{\nabla \cdot \langle \rho_\beta \omega_{A\beta} \mathbf{v}_\beta \rangle}_{(b)} = \underbrace{\nabla \cdot \langle \rho_\beta D_{A\beta} \nabla \omega_{A\beta} \rangle}_{(c)} - \underbrace{\frac{1}{V} \int_{A_{\beta\sigma}} \mathbf{n}_{\beta\sigma} \cdot \rho_\beta \omega_{A\beta} (\mathbf{v}_{A\beta} - \mathbf{w}) dA}_{(d)} \quad (15)$$

The different terms (a), (b), (c) and (d) express *accumulation*, *convection*, *diffusion* and *phase exchange* terms, respectively. In the same manner, we define the intrinsic average of the mass fraction as,

$$\Omega_{A\beta} = \langle \omega_{A\beta} \rangle^\beta = \varepsilon_\beta^{-1} \langle \omega_{A\beta} \rangle = \frac{1}{V_\beta} \int_{V_\beta} \omega_{A\beta}(\mathbf{r}) dV$$

and the superficial average of the velocity gives:

$$\mathbf{V}_\beta = \langle \mathbf{v}_\beta \rangle = \varepsilon_\beta \langle \mathbf{v}_\beta \rangle^\beta = \frac{1}{V} \int_{V_\beta} \mathbf{v}_\beta(\mathbf{r}) dV$$

where  $\varepsilon_\beta$  is the volume fraction of the  $\beta$ -phase,  $\mathbf{V}_\beta$  is the filtration velocity and  $\langle \mathbf{v}_\beta \rangle^\beta$  is the  $\beta$ -phase intrinsic average velocity. After several assumptions and some mathematical treatment of the different equations we have the following control equations for the diffuse interface model (DIM) [12]:

$$\varepsilon_\beta \rho_\beta^* \frac{\partial \Omega_{A\beta}}{\partial t} + \rho_\beta^* \mathbf{V}_\beta \cdot \nabla \Omega_{A\beta} = \nabla \cdot (\varepsilon_\beta \rho_\beta^* \mathbf{D}_{A\beta}^* \cdot \nabla \Omega_{A\beta}) + \rho_\beta^* \alpha (1 - \Omega_{A\beta}) (\omega_{eq} - \Omega_{A\beta}) \quad (16)$$

$$\frac{\partial \varepsilon_\beta \rho_\beta^*}{\partial t} + \nabla \cdot (\rho_\beta^* \mathbf{V}_\beta) = \rho_\beta^* \alpha (\omega_{eq} - \Omega_{A\beta}) \quad (17)$$

and

$$-\rho_\sigma \frac{\partial \varepsilon_\sigma}{\partial t} = \rho_\sigma \frac{\partial \varepsilon_\beta}{\partial t} = \rho_\beta^* \alpha (\omega_{eq} - \Omega_{A\beta}) \quad (18)$$

where  $\mathbf{D}_{A\beta}^*$  is the macroscopic diffusion/dispersion coefficient,

$$\rho_\beta^*: \text{ such that } \langle \rho_\beta \omega_{A\beta} \rangle = \varepsilon_\beta \rho_\beta^* \Omega_{A\beta}$$

and  $\alpha$  is the exchange term between the two phases. The macroscopic diffusion/dispersion coefficient and the exchange term are obtained by solving the closure problem characterized by two boundary value problems.

The determination of the two "mapping variables" (closure variables) during upscaling requires solving two additional boundary value problems. The resolution of these issues is carried out for representative unit cells. These are not unique, as shown in the Figure 5.

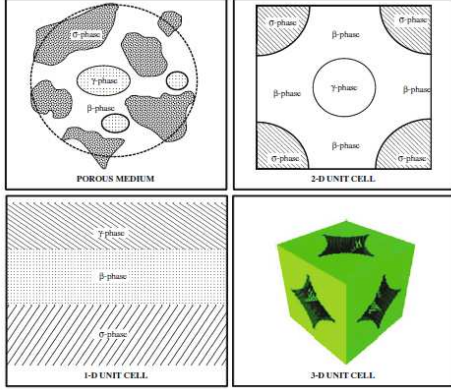


Fig. 5: Examples of 1D, 2D and 3D unit cells [15]

For example, if we assume that the deviation of the mass fraction of species A is as following:

$$\tilde{\omega}_{A\beta} = \mathbf{b}_\beta \cdot \nabla \Omega_{A\beta} + s_\beta (\omega_{eq} - \Omega_{A\beta})$$

The two closure variables are  $\mathbf{b}_\beta$  and  $s_\beta$ .

Solving two boundary value closure problems allows us to express the macroscopic effective values according to their value at the microscopic scale. In other words, the physical properties at the macroscopic level are not "phenomenological macroscopic" but built on the basis of physical properties observed-defined at the microscopic scale.

Let's recall for example the effective macroscopic diffusion tensor  $\mathbf{D}_{A\beta}^*$ , the macroscopic effective exchange coefficient  $\alpha$  and the effective density  $\rho_\beta^*$ :

$$\mathbf{D}_{A\beta}^* = D_{A\beta} \left( \mathbf{I} + \varepsilon_\beta^{-1} \frac{1}{V} \int_{A_{\beta\sigma}} (\mathbf{n}_{\beta\sigma} \mathbf{b}_\beta) dA \right) - \varepsilon_\beta^{-1} \langle \mathbf{b}_\beta \tilde{\mathbf{v}}_\beta \rangle \quad (19)$$

$$\alpha = \frac{1}{V} \int_{A_{\beta\sigma}} \frac{\rho_\beta}{(1 - \omega_{eq})} D_{A\beta} (\mathbf{n}_{\beta\sigma} \cdot \nabla s_\beta) dA \quad (20)$$

$$\rho_\beta^* = \frac{1}{\varepsilon_\beta \Omega_{A\beta}} \langle \rho_\beta \omega_{A\beta} \rangle$$

On the basis of microscopic considerations and some assumptions described above, we finally get the macroscopic transport equation.

The term involving the exchange coefficient  $\alpha$  comes into the equation as a source term for the phase  $\beta$ . We observed that when the saturation in a material point is reached then:

$$\begin{aligned} \omega_{eq} &= \Omega_{A\beta} \\ \Rightarrow \frac{\partial \varepsilon_\beta}{\partial t} &= 0 \Leftrightarrow \varepsilon_\beta = Cte \end{aligned}$$

Although we have formulated the problem the "most accurately," we have at present no macroscopic model unless we specify some specific unit cell in order to determine its actual properties. We have adopted in our modeling macroscopic literature values for diffusion.

In the case of DIM use, i.e., not a real porous medium problem, the choice of the exchange coefficient  $\alpha$  expression depending on the porosity is arbitrary. It must, however, be observed a nullity condition when the material point is considered strictly in the fluid phase or strictly in the solid phase. This is illustrated in Figure 6.

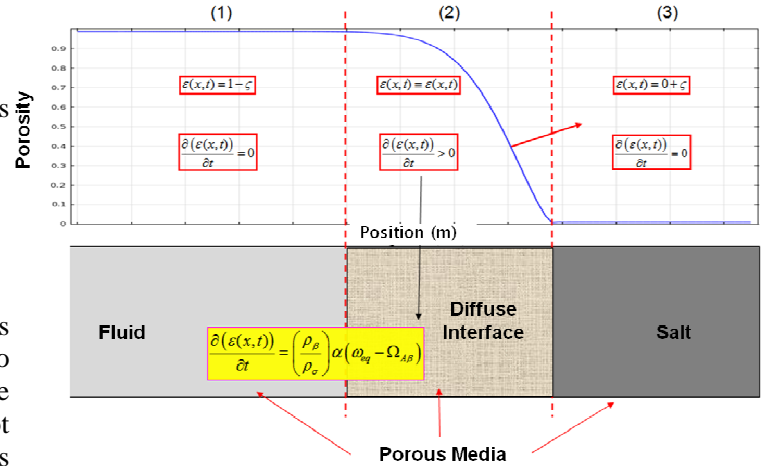


Fig. 6: Porous domains : "fluid"-interface-solid and expression of the volume fraction  $\varepsilon$

We must underline that, in the DIM model, there is no "pure liquid phase" (Figure 6) since  $\varepsilon_\beta$  is used continuously to represent the fluid as well as the solid regions. Therefore, the Navier-Stokes equations are no longer suitable for this situation. Instead, we can adopt a Darcy-Brinkman model [2] to take the place of Navier-Stokes equations for the momentum equations,

$$\frac{\mu_\beta(\Omega_{A\beta})}{\varepsilon_\beta} \Delta \mathbf{V}_\beta - (\nabla P_\beta - \rho_\beta^* \mathbf{g}) - \mu_\beta(\Omega_{A\beta}) \mathbf{K}^{-1} \cdot \mathbf{V}_\beta = 0 \quad (21)$$

where  $\mathbf{K}$  is a function of  $\varepsilon_\beta$ . The Darcy-Brinkman equation will approach Stokes equation when  $\mathbf{K}$  is very large and will simplify to Darcy's law when  $\mathbf{K}$  is very small. If inertia terms are not negligible, a similar Darcy penalization of Navier-Stokes equations may be used.

### 3 NUMERICAL MODELLING

For numerical simulations, COMSOL™ is used for both ALE and DIM simulations. In order to use the DIM model more freely and effectively, we also developed our own code for the DIM simulations. Our own code adopts a Finite Volume difference method for discretization with an upstream scheme to stabilize advection terms.

#### 3.1 Example of a plane flow problem

For the simulations, a 2D geometry is firstly adopted as illustrated in Figure 7. Pure water is injected with a constant velocity ( $U_0$ ) into a channel whose walls are formed by two parallel salt blocks, resulting in the dissolution of the solid walls. The calibrated (for salt) parameters used in this modeling are illustrated in Table 1.

Table 1. The parameters used for simulation examples.

Parameter	Value	Unit
$\rho_\sigma$	$2.165 \times 10^3$	$Kg/m^3$
$\rho_\beta$	$1.0 \times 10^3(1 + 0.7385\omega_\beta)$	$Kg/m^3$
$\mu_\beta$	$1.2 \times 10^{-3}$	$Kg/ms$
$L$	$2 \times 10^{-3}$	$m$
$D_{salt}$	$1.3 \times 10^{-9}$	$m^2/s$
$\omega_{eq}$	0.27	-
$U_0$	<i>under choice</i>	$m/s$

Concerning the velocity, if  $U_0 = 10^{-6} \text{ ms}^{-1}$ , the Péclet number (Pe) calculated as  $Pe = U_0 L/D_{salt}$  ( $D_{salt}$  rock salt diffusion coefficient in water) is close to unity, i.e., same importance of diffusion and advection mechanisms. The ALE module is adopted for original solid/liquid dissolution simulations, while the second method is the Darcy-scale DIM method.

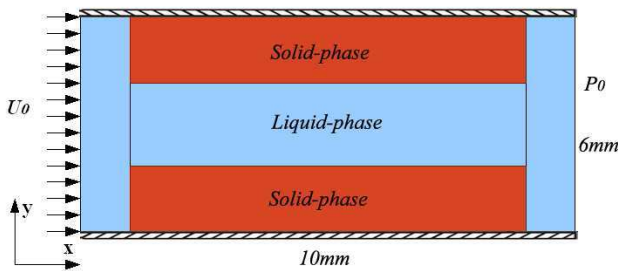


Fig. 7. The 2D geometry used for the simulation examples.

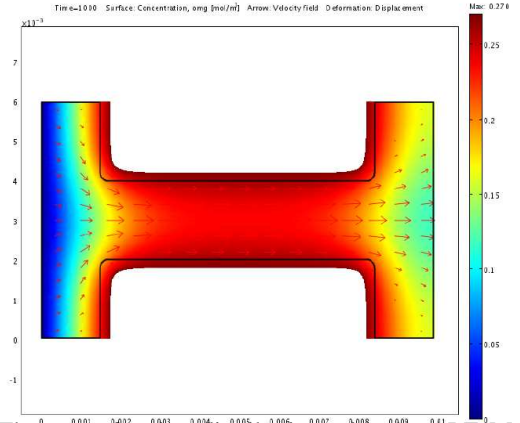


Fig. 8. The mass fraction distribution with the ALE Module and Navier-Stokes equations at time  $t = 1000s$  ( $Pe = 0.1$ ) [13]

Figure 8 and 9 show that the solid/liquid interfaces have moved due to dissolution. A larger interface displacement can be seen for the larger Péclet number, as the concentration gradients are obviously steeper.

For the same reason, the interface displacement is larger near the inlet than near the outlet.

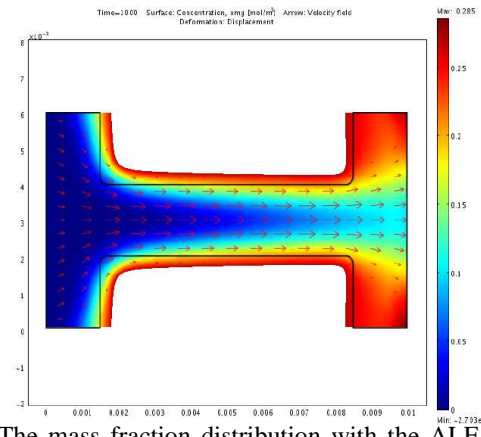


Fig. 9. The mass fraction distribution with the ALE Module and Navier-Stokes equations at time  $t = 1000s$  ( $Pe = 10$ ) [13]

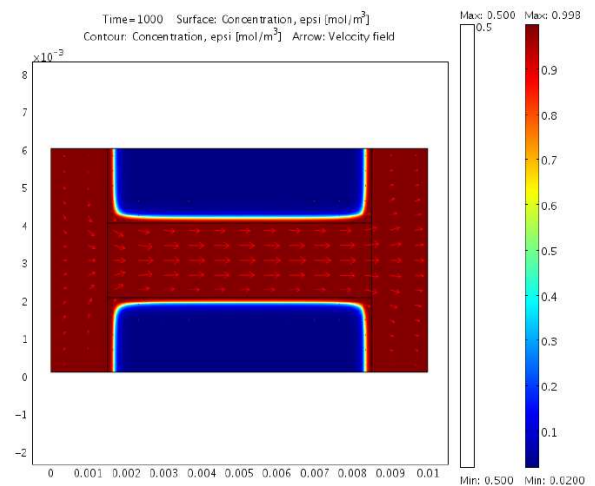


Fig. 10. The volume fraction (porosity)  $\varepsilon_\beta$  distribution at 1000 s using DIM model ( $Pe = 0.1$ ) [13].

Figures 10 and 11 show sharp volume fraction gradients around the interfaces. The comparison between the different figures reveals that one can obtain similar mass fraction distributions and interface displacements by using either the ALE module or the DIM model. As a better explicit comparison, Figure 12 compares the interface displacement along the y-direction versus  $x$  (for DIM, we utilize the lines where  $\varepsilon_\beta$  equals 0.5 to represent the interface location). The comparison shows that the results from the different models reach a tolerable agreement.

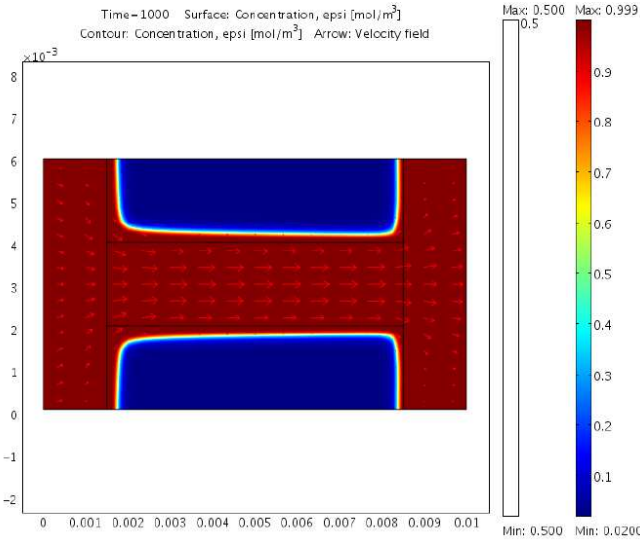


Fig. 7. The volume fraction (porosity) distribution at 1000s using DIM model ( $Pe = 10$ ) [13].

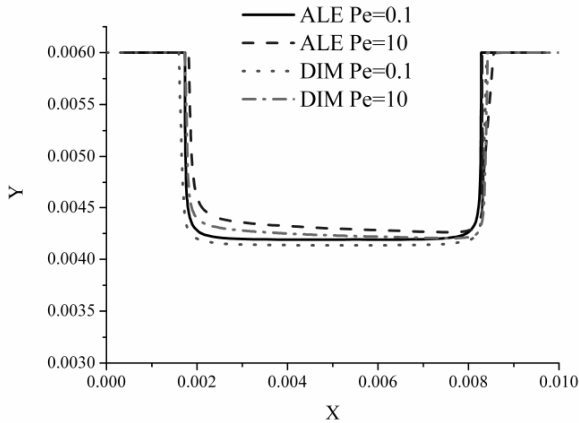


Fig. 12. Comparison of the interface shape at  $t = 1000s$  between ALE and DIM [13].  $Y$  and  $X$  are the coordinate of the cross section of the interface.

It has to be reminded that, for the diffuse interface model, the choice of the exchange term,  $\alpha$ , in an appropriate range will not severely influence the evolution of dissolution, because the “diffuse interface” is not a real interface: with larger  $\alpha$  numbers the

interface will become thinner while with smaller  $\alpha$  numbers it will become thicker. This changes the concentration profile near the interface rather than the total exchanged mass.

Whenever density variation is present in the fluid phases, the gravity (buoyancy force) can play an important role in mass and heat transports, through the mechanism of natural convection. In our case, the dissolution of the salt walls results in higher concentrations around the interface than in other fluid regions. Therefore, it makes sense to study the influence of gravity effects upon the dissolution and fluid flow. To characterize the gravity effects for dissolution problem, one can refer to the Rayleigh number,  $Ra$ , which is defined as the ratio of buoyancy forces to mass and momentum diffusivities.

$$Ra = \frac{\Delta\rho_{max} |g| K_{max} L}{\mu_\beta D_\beta}$$

This natural convection phenomenon, often called salt fingering, is well illustrated by Figures 13 and 14.

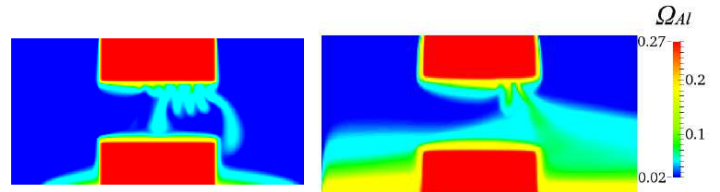


Fig. 13: Examples of concentration plumes for a 2D simulation with gravity at time 100 s and 1000 s and salt block size 8 mm.

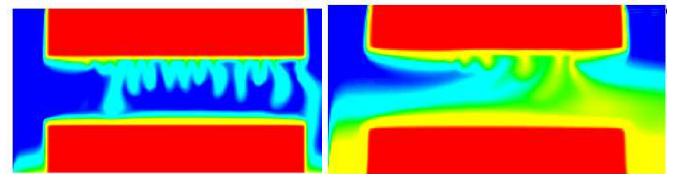


Fig. 14: Examples of concentration plumes for a 2D simulation with gravity at time 100 s and 1000 s and salt block size 16 mm. (color scale bar as in Fig. 13).

We show that the shape on the top of the channel has lost its regularity and the wavy shape is due to physical Rayleigh convective instability which induces a vortex motion of fluid particles. The heavy fluid (more saturated) goes downward and increases the dissolution upward.

### 3.2 Axisymmetrical cavity

This section is devoted to the numerical modeling of an experimental “large scale” dissolution process. The goal is to show the ability of the DIM method to tackle difficult problems with geometry singularities and natural convective components.

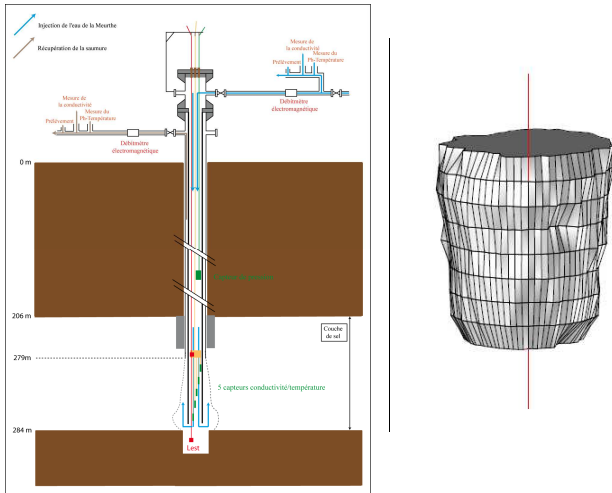


Fig. 15. Illustration of the experimental salt rock dissolution process (right) and shape of the cavity after 12 days (right) [16].

A concentric leaching well was drilled to the final depth (The salt layer is located at about 280 meters depth). The tubing is constituted by two concentric tubes. Then fresh water was injected through the central annulus during 12 days [16]. This method is known as *direct leaching process*. The inlet flow is 3 m<sup>3</sup>/h during 4 days followed by 1.5 m<sup>3</sup>/h during 8 days [16]. The Figure 16 depict the experimental setting and the final shape of the cavity (obtained by sonar).

We shows below some results of our numerical modeling. Figure 16 shows the axisymmetric mesh and model.

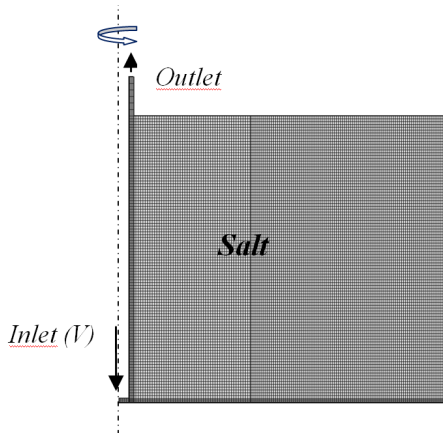


Fig. 16. Geometry and boundary condition for the cavity dissolution model.

The deduced inlet velocity is 8 cm/s during 4 days and then 4 cm/s during 8 days.

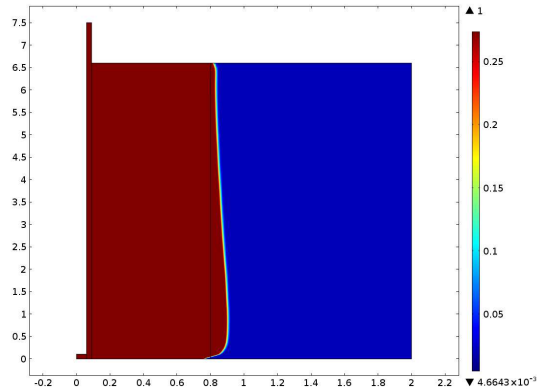


Fig. 17. Isovalue of the porosity after 4 days. (void for unity).

From the Axisymmetrical shape of the cavity the computed dissolved volume is around 12 m<sup>3</sup> (the measured in-situ is around 11 m<sup>3</sup>)

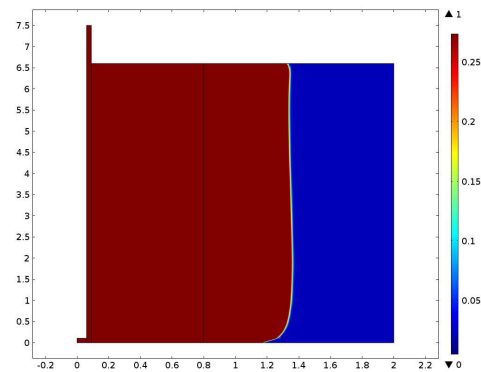


Fig. 18. Isovalue of the porosity after 12 days (void for unity).

From the axisymmetrical shape of the cavity the computed dissolved volume is around 38 m<sup>3</sup> (the measured in-situ is around 40 m<sup>3</sup>).

In Figure 19 it can be observed the time evolution of a *not sharp but the diffuse* fluid-salt interfaces.

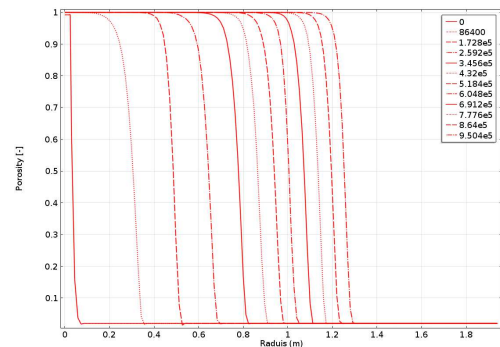


Fig. 19 . Examples of the distribution of the porosity at a line located at the middle of the model and at several times (1 to 12 days).

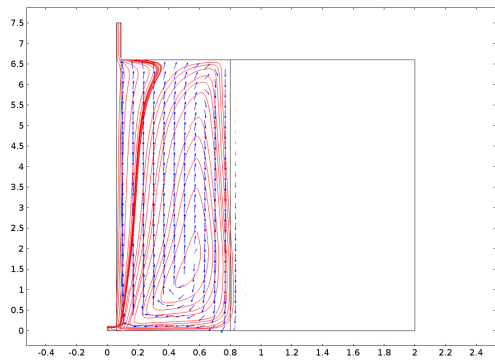


Fig. 20 . Streamlines and vectors field after 4 days

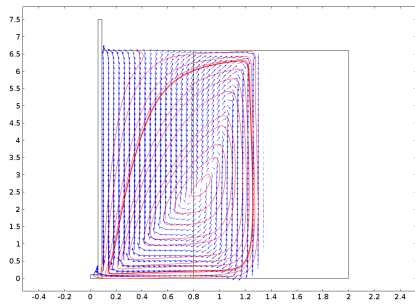


Fig. 21. Streamlines and vectors field after 8 days

Figures 20 and 21 gives illustrations of the streamlines and fluid velocity field at two time steps. We can show the effect of the natural convection.

The numerical method was extended to a three-phases (gas-liquid-solid) [14] problems and to other dissolving matter. For gypsum, for instance, it dissolves in flowing water about one hundred times more rapidly than limestone, but at only about one thousandth the rate of halite. Figures 22 and 23 show the shape of the cavity in a gypsum medium, using the same hydrodynamic conditions as above for the salt.

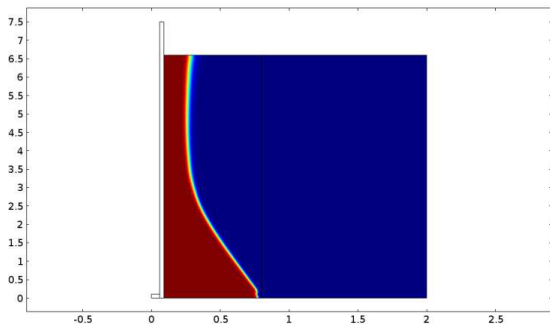


Fig. 22. Isovalue of the porosity in gypsum after 3 years (void in red)

The two examples (Figures 23 and 24) are for a small gypsum layer thickness (4.4 m) and an inlet velocity of 1 cm/s.

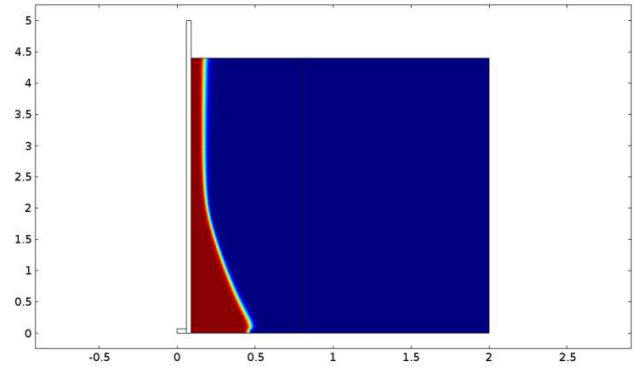


Fig. 23. Isovalue of the porosity in gypsum after 10 years (void in red)

We observe that the very low dissolution rate for gypsum material and the cavity shape which is very different from that obtained with salt. The natural convection is very small due to the low solubility of gypsum. We have extended our two-phase DIM to three phases [14]. In the case of multi-phase (three phases) the air phase occurring in many groundwater or mining problems is taken into account. In order to improve computation the DIM method is used with an AMR (Adaptative Mesh Refining) [14]. Figures 24 and 25 give an illustration of the numerical simulations.

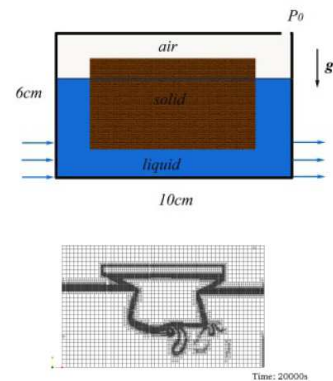


Fig. 24. Example of a three phase-AMR result [14] .

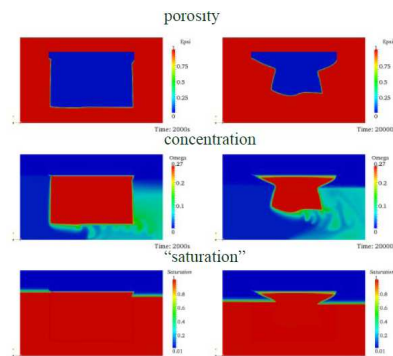


Fig. 25. Porosity, salt concentration and saturation after  $2 \cdot 10^4$  s [14].

## 4 CONCLUSION

For simulations of solid-liquid dissolution processes, one can use either explicit treatment methods (e.g. ALE in this paper) or diffuse interface methods (a local non-equilibrium DIM in this paper).

The ALE is not suitable for simulating the problems with complex interfaces, e.g., sharp angles, porous media, as it relies strongly on the mesh shape. In the contrary, the DIM is more suitable to simulate dissolution problems, as the whole domain is composed by a phase field (volume fraction of liquid phase in this paper). In this paper a local non-equilibrium diffuse interface model based on a porous medium theory is extended to study dissolution problems, with density variations taken into account.

As the DIM considers the density variations, simulation with gravity becomes available. For a dissolution problem with high concentration gradients, for example, NaCl dissolved into water, Raleigh-Bénard physical instabilities can be aroused under this situation. As expected, examples show that the physical instability is enhanced by increasing the Ra number. Unstable flows, salt fingers, and dissolving interface induced wavelets are observed. Actually, the physical instability dynamic is not only controlled by the Ra number, but also related to the Pe number [13]. In the space Ra-Pe, interactions have been well documented [13] and the trends of the influences, show extremely complicated patterns. The physical instability during dissolution processes is certainly a problem which has to be looked at in further study.

Furthermore, the potential advantage of using the diffuse interface model is that it enables us to introduce automatic remeshing algorithms, such as AMR algorithm, which can greatly improve the calculation speed and accuracy, since very fine meshes are required near the interface. The method has been extended to multi-phase problems and to gypsum material. DIM method is so robust that it can perform successfully numerical dissolution for a wide range of dissolution rates. Our ultimate goal is to strongly couple (two ways coupling) the dissolution process with the mechanical behavior of the dissolving formation for instance.

## References

1. Anderson, D.M. & McFadden, G.B. 1998. Diffuse-interface methods in fluid mechanics. *Annual Review of Fluid Mechanics*, 30:139–165.
2. Brinkman, H.C. 1947. A calculation of the viscous force exerted by a flowing fluid on a dense swarm of particles. *Appl. Sci. Res.*, 1:27–34.
3. Collins, J.B. & Levine, H. 1985. Diffuse interface model of diffusion-limited crystal growth. *Phys. Rev. B*, 31: 6119–6122.
4. Donea, J., Giuliani, S. & Halleux, J.P. 1982. An arbitrary lagrangian-eulerian finite element method for transient dynamic fluid-structure interactions. *Computer Methods in Applied Mechanics and Engineering*, 33:689–723.
5. Golfier, F., Zarcone, C., Bazin, B., Lenormand, R., Lasseux, D. & Quintard, M. 2002. On the ability of a darcy scale model to capture wormhole formation during the dissolution of a porous medium. *Journal of Fluid Mechanics*, 457:213–254.
6. Leo, P.H., Lowengrub, J.S., & Jou, H.J. 1998. A diffuse interface model for microstructural evolution in elastically stressed solids. *Acta Mater.*, 46:2113–2130.
7. Luo, H., Quintard, M. Debenest, G. & Laouafa, F. 2011. Properties of a diffuse interface model based on a porous medium theory for solid-liquid dissolution problems. *Computational Geosciences*, Submitted.
8. Quintard, M. & Whitaker, S. 1994. Transport in ordered and disordered porous media 1: The cellular average and the use of weighing functions. *Transport in Porous Media*, 14:163–177.
9. Quintard, M. & Whitaker, S. 1994. Convection, dispersion, and interfacial transport of contaminant: Homogeneous porous media. *Advances in Water Resources*, 17:221–239.
10. Quintard, M. & Whitaker, S. 1999. Dissolution of an immobile phase during flow in porous media. *Ind. Eng. Chem. Res.*, 38:833–844.
11. Taylor, R. & Krishna, R. 1993. *Multicomponent Mass Transfer*. Wiley-Interscience.
12. Whitaker, S. 1999. *The Method of Volume Averaging*. Kluwer Academic Publishers.
13. Luo, H., Quintard, M. Debenest, G. & Laouafa, F. 2012. Properties of a diffuse interface model based on a porous medium theory for solid-liquid dissolution problems. *Computational Geosciences*, 16(4), 913-932
14. Luo, H., Laouafa, F., Guo, J., Quintard, M. 2014. Numerical modeling of three-phase dissolution of underground cavities using a diffuse interface model. *Int. J. Numer. Anal. Meth. Geomech* DOI:10.1002 / nag.2274.
15. Courtelieiris, F. A., Delgado, J.M.P.Q. 2012. *Transport porocess in Porous Media*. Springer
16. A. Charmoille, X. Daupley and F. Laouafa. 2012. *Analyse et modélisation de l'évolution spatio-temporelle des cavités de dissolution*. Report DRS-12-127199-10107A. INERIS